Journal of
Manufacturing and Materials Processing

MDPI

Article

Effect of Lattice Structure on Mechanical Properties of Ti-6Al-4V-Ta Alloy for Improved Antibacterial Properties

Anel Zhumabekova [1], Malika Toleubekova [2], Tri Thanh Pham [2], Didier Talamona [1,*] and Asma Perveen [1,*]

[1] Department of Mechanical and Aerospace Engineering, School of Engineering & Digital Sciences, Nazarbayev University, Astana 010000, Kazakhstan; anel.zhumabekova@nu.edu.kz
[2] Department of Biology, School of Sciences and Humanities, Nazarbayev University, Astana 010000, Kazakhstan; malika.toleubekova@nu.edu.kz (M.T.); tri.pham@nu.edu.kz (T.T.P.)
* Correspondence: didier.talamona@nu.edu.kz (D.T.); asma.perveen@nu.edu.kz (A.P.)

Abstract: This study investigates the effect of a tantalum addition and lattice structure design on the mechanical and antibacterial properties of Ti-6Al-4V alloys. TPMS lattice structures, such as Diamond, Gyroid, and Primitive, were generated by MSLattice 1.0 software and manufactured using laser powder bed fusion (LPBF). The results indicate that Gyroid and Primitive structures at a 40% density exhibit superior ultimate compressive strength, which closely emulates bone's biomechanical properties. To be precise, adding 8% tantalum (Ta) significantly increases the material's elastic modulus and energy absorption, enhancing the material's suitability for dynamic load-bearing implants. Nevertheless, the Ta treatment reduces bacterial biofilm formation, especially on Gyroid surfaces, suggesting its potential for infection management. Overall, all findings provide critical insights into the development of advanced implant materials, contributing to the fields of additive manufacturing, materials science, and biomedical engineering and paving the way for improved patient outcomes in orthopedic applications.

Keywords: additive manufacturing; selective laser melting; Ti6Al4V; Ti6Al4V-Ta; triply periodic minimal surface; antibacterial responses

Citation: Zhumabekova, A.; Toleubekova, M.; Pham, T.T.; Talamona, D.; Perveen, A. Effect of Lattice Structure on Mechanical Properties of Ti-6Al-4V-Ta Alloy for Improved Antibacterial Properties. *J. Manuf. Mater. Process.* **2024**, *8*, 133. https://doi.org/10.3390/jmmp8040133

Academic Editor: Panagiotis Stavropoulos

Received: 27 May 2024
Revised: 20 June 2024
Accepted: 20 June 2024
Published: 26 June 2024

1. Introduction

Recent advancements in biomedical titanium alloys have significantly enhanced the performance and applicability of medical implants, crucial for improving patient outcomes and quality of life. Biocompatibility remains a fundamental requirement, with current research focusing on incorporating elements such as molybdenum (Mo), tantalum (Ta), and chromium (Cr) to enhance the interaction between the implants and biological tissues [1–3]. These elements improve cell adhesion and reduce inflammation, ensuring harmonious integration with human tissues. The development of specialized alloys like shape memory titanium alloys, β-type titanium alloys, and high-entropy titanium alloys has also progressed, offering them enhanced mechanical properties, including increased strength and improved fatigue resistance. Notably, the Ti-24Nb-4Zr-8Sn alloy, prepared through laser powder bed fusion (LPBF), exemplifies the advancements in alloy design, providing near-full density parts suitable for use in acetabular prostheses [4]. Additionally, surface modification techniques such as anodization, micro-arc oxidation, and bioactive coatings have been extensively studied to enhance their biocompatibility, wear resistance, and corrosion resistance, contributing to the long-term effectiveness and safety of titanium-based implants [5–7].

Additive manufacturing (AM) technologies, including LPBF and Electron Beam Melting (EBM), have revolutionized the fabrication of titanium-based biomedical implants, enabling precise and complex designs that enhance osseointegration and mechanical compatibility [1,8]. These technologies allow for the creation of tailored structures that meet individual patient needs, thereby improving implant stability and reducing the risk of

complications. For instance, Ti-Ta alloy lattice structures produced using laser powder bed fusion (L-PBF) exhibit superior fracture energy and mechanical performance, making them highly suitable for orthopedic applications [9]. Furthermore, Nitinol, a nickel–titanium alloy known for its superelasticity and shape memory effects, has emerged as a significant material for various medical devices, including orthopedic implants and vascular stents [10]. Ongoing research aims to optimize Nitinol's processing techniques to further improve its mechanical properties and corrosion resistance, ensuring its durability and functionality in clinical applications [11]. These advancements in alloy design, surface modification, and additive manufacturing technologies are paving the way for the next generation of more effective, durable, and biocompatible medical implants.

Recent advancements in 3D printing, particularly in the creation of lattice structures, have revolutionized various industries through the development of sophisticated additive manufacturing (AM) technologies. Notable progress has been made in Powder Bed Fusion (PBF), Direct Energy Deposition (DED), and the integration of AM with traditional manufacturing methods. PBF technologies, including Selective Laser Sintering (SLS) and selective laser melting (SLM), have enabled the precise fabrication of complex geometries, improving mechanical properties by optimizing processing parameters. Similarly, DED technologies like Laser-Engineered Net Shaping (LENS) and Wire and Arc Additive Manufacturing (WAAM) facilitate the production and repair of large-scale components, although they still face challenges in terms of surface finish and accuracy [12,13]. Hybrid methods, combining rapid prototyping with powder metallurgy, have also emerged, allowing the creation of intricate lattice patterns previously unattainable with conventional techniques [14]. Nevertheless, Perez's exploration of stiffening near-net-shape functional parts through crystallographic texture control and laser beam shaping provides a future path to use AM with improved mechanical properties [15–17]. For instance, their study found that non-Gaussian beam profiles significantly influence the mechanical properties of IN718 during laser powder bed fusion (LPBF) [17]. Gaussian beams led to higher porosity and deeper melt pools with lamellar structures, whereas ring beams produced more uniform melt pools with a consistent crystalline orientation. Nevertheless, although IN718 was studied in the investigations of crystallographic texture control and laser beam shaping, other materials can be investigated using the same methodology. In addition to this, the post-processing and finishing of lattice structures have been investigated by electrical discharge machining (EDM) [18]. That study showed the great promise of IN718 through-hole drilling in analyzing the variability in the dimensions of the features caused by the periodically open pores.

Collaborative innovations have further propelled the field, with partnerships such as Farsoon Technologies, Hyperganic, and BASF Forward AM developing the Ultrasim 3D Lattice Engine. This platform simplifies lattice structure production, democratizing access to advanced AM capabilities [19]. In terms of biomedical applications, researchers at the City University of Hong Kong have enhanced the strength of 3D-printed polymeric lattice components through partial carbonization, making them suitable for critical applications like coronary stents [20]. The aerospace and automotive industries benefit from technologies like the 3D Cocooner by Festo, which creates bionic lattice structures with high tensile strength and structural integrity [20]. These advancements demonstrate the transformative potential of 3D printing in producing lightweight, robust components across various sectors.

Ti-6Al-4V is a widely used titanium alloy in biomedical applications due to its excellent mechanical properties, corrosion resistance, and biocompatibility. This alloy, composed of titanium with 6% aluminum and 4% vanadium, offers high tensile strength and fatigue resistance, making it ideal for load-bearing implants such as hip and knee replacements, dental implants, and spinal fixation devices [21]. Its modulus of elasticity, closer to human bone, reduces stress shielding effects, while its stable oxide layer protects against corrosion, enhancing implant longevity [21]. However, challenges remain, particularly in improving osseointegration and preventing postoperative infections [22]. Research has focused on

advanced surface modification techniques, such as sand-blasting large-grit acid-etching (SLA) and silver nanoparticle coatings via electron beam evaporation (EBE), to enhance the alloy's bioactivity and antibacterial properties [22]. While these modifications show promise in promoting better bone cell attachment and reducing bacterial colonization, optimizing these coatings for long-term stability and effectiveness while maintaining biocompatibility is crucial [22]. Thus, ongoing research aims to overcome these limitations, developing next-generation implants with enhanced performance and reliability in clinical settings. While aluminum (Al) and vanadium (V) ions are widely accepted as industry standards, new research has raised serious concerns about their potential toxicity in the body [23,24]. Instead of these harmful elements, alloying with Niobium (Nb), Tantalum (Ta), or Zirconium (Zr) has been attempted recently [25–27]. As a result, these materials have been found to perform better than Ti-6Al-4V, which has motivated researchers to create new biocompatible metals with different alloying components.

Tantalum (Ta) is gaining interest because of its exceptional biocompatibility and excellent resistance to corrosion; nonetheless, its applications are confined to mostly surface coatings due to its high cost and machining difficulty [28]. For biomedical applications, it is a promising alloying complement to pure titanium. When standard irregular tantalum powders are utilized, mixing Ta and Ti powders is an effective technique to lower the material's cost and increase the flowability of the powder mixture [29]. Furthermore, tantalum can stabilize titanium's β, which is advantageous for biomedical applications (i.e., creating a low modulus and high strength) [30]. Sing et al. [28] report that, compared to commercially pure titanium (cp-Ti), titanium–tantalum (Ti–Ta) alloys exhibit higher relative strength (for comparable stiffness) and a lower elastic modulus, as well as superior corrosion resistance and superior biocompatibility properties. However, instead of using pure Ti, there are also some upcoming investigations around Ti6Al4V-Ta attempting to improve its mechanical properties. There is an ongoing investigation on the creation of Ti-6Al-4V by adding Ta at different weight ratios (0%, 2%, 4%, and 6% of Ta) [30]. The results showed that strength and ductility increase when Ta is added to the Ti-6Al-4V alloy. The alloy Ti-6Al-4V–4Ta has a weaker selection of α-variants and the most consistent basketweave microstructure. A four percent weight addition of Ta improves its mechanical performance significantly (Ultimate Tensile Strength (UTS)—1042 MPa, yield strength (YS)—956 MPa, and elongation—10.8%) compared to Ti-6Al-4V–0Ta without Ta. These improved mechanical properties are ascribed to a higher dislocation density, solid Ta element solution, weaker α-variants selection, and refined microstructure. This exploration of integrating tantalum into titanium alloys (Ti-6Al-4V-Ta) enhances their mechanical properties and biocompatibility. The addition of tantalum significantly improves the strength, ductility, and antibacterial properties of the alloy, making it promising for medical implants. As Perez's contributions provide a comprehensive pathway for using SLM and LPBF to create advanced materials with tailored properties, improve material performance, and expand their application in critical fields, Ti-6Al-4V-Ta has a chance to be the future investigated material after IN718 [15–17]. Nevertheless, improving the post-processing and finishing of samples made of Ti-6Al-4V-Ta, as in the study of Singh et al. [18], is an advantage for future investigations.

This research aims to estimate the mechanical and biological response properties of the Ti-6Al-4V-Ta alloy. First of all, this study investigates the mechanical performance and energy absorption characteristics of different lattice structures made of Ti-6Al-4V and Ti-6Al-4V-Ta alloys. This study identifies the elastic moduli, yield strengths, energy absorption values, and energy absorption efficiencies of various stretch- and bending-dominated lattice structures under quasistatic compression. Finally, the biomedical compatibility of Ti-6Al-4V and Ti-6Al-4V-Ta lattice alloys will be assessed via the adhesion of bacteria on the LPBF-printed surface.

2. Materials, Methodology, and Equipment

This section covers the design and manufacturing processes of the chosen material, the mechanical analysis and characterization of printed and tested material, and the bacteria adhesion methodology for the Ti-6AL-4V and Ti-6AL-4V-Ta alloys.

2.1. Lattice Structures' Design

The design of the lattice specimens was mainly implemented using MSLattice for triply periodic minimal surface (TPMS) structures. MSLattice uses Matlab's code but simplifies the work: only the type of TPMS lattice structure, density, unit cell size, height, and width need to be entered. After that, it provided the .stl files of the needed TPMS structures for this research. A literature review showed that Diamond, Gyroid, and Primitive (Figure 1) lattice structures perform best overall in energy absorption and contain porosity and stiffness similar to human bones [23–27].

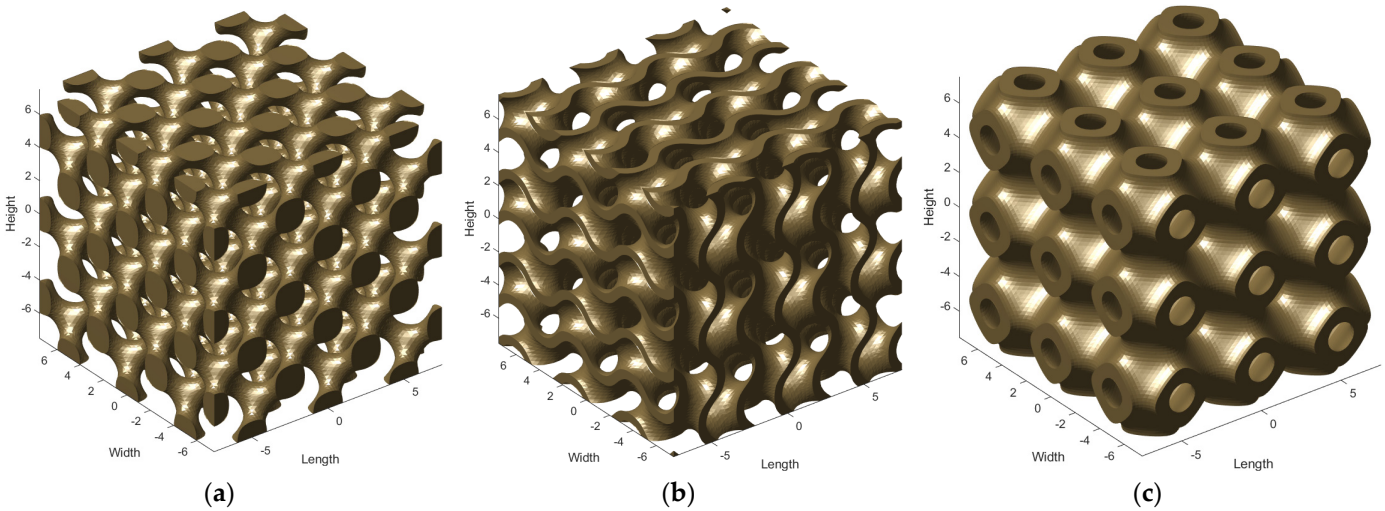

Figure 1. Types of lattice structures that were investigated: (**a**) Diamond; (**b**) Gyroid; (**c**) Primitive.

In this proposed research, 30–40% density and a unit cell size (UCS) of 3 mm for Ti-6Al-4V and Ti-6Al-4V-Ta structures were investigated. Table 1 represents the density and size of the lattice structures generated in MSLattice.

Table 1. The density and size of the lattice structures generated in MSLattice made of Ti-6Al-4V and Ti-6Al-4V-Ta.

Models	Density, %	UCS, mm	Height, mm	Width, mm
Diamond	30, 35, 40	3	15	15
Gyroid	30, 35, 40	3	15	15
Primitive	30, 35, 40	3	15	15

2.2. LPBF Process Parameters and Manufacturing

The specimens used in this study were LPBF-printed Ti-6Al-4V ELI and Ti-6Al-4V-Ta alloys. The powder Ti-6Al-4V ELI, with a grade size of 20–53 µm, was acquired from Sino-Euro Materials of Xi'an Co, Ltd. (Sino-Euro, Xi'an, China), a Northwest Institute for Non-ferrous Metal Research division. Also, as an alloying option for this study, Ti-6Al-4V powder was mixed with Ta powder. It creates a mixture of 92 wt% Ti-6Al-4V and 8 wt% pure tantalum (Ta). The Ta powder has a grain size of 15-53 µm and was bought from Luoyang Tongrun Info Technology Co., Ltd. (Luoyang, Henan, China). A mixture machine Inversina 2L Tumbler Mixer which is bought from Bioengineering AG (Wald, Switzerland) was used to mix the powders. The Ti–6Al-4V-Ta powder was tumbled and mixed for 7.5 h at 60 rpm.

A Renishaw AM 400 (Renishaw plc, Staffordshire, United Kingdom) was utilized to produce the specimens using the LPBF principle. The process parameters selected were the default Renishaw suggestions, chosen from the software library for Ti-6Al-4V. Hence, all samples were manufactured with a laser power of 200 W, hatch spacing of 0.08 mm, scanning speed rate of 1112 mm/s, and layer thickness of 0.03 mm. These LPBF-printing process parameters were used for both alloying options made of Ti-6Al-4V and Ti-6Al-4V-Ta. All printing was carried out using the reduced build volume (RBV) platform.

2.3. Lattice Structure Characterization

Compression tests were performed on the TPMS lattice structures highlighted in Table 1. An image of the test setup, Figure A1, can be found in Appendix A. During the test, a specimen is compressed from the up to the down position, as seen in Figure A1, and a preload of up to 50 N is applied to fix the samples before the test run. The compression tests were conducted at a strain rate of 1 mm/min until the ultimate compression strength value was reached. After the test, other mechanical characteristics were investigated such as stress–strain, energy absorption, and its efficiency, plateau stress.

The values of the stress (represented by σ) and strain (represented by ε) are determined based on factors such as the force applied by the compression plate to the lattice (F), the initial area of the lattice base (A_0), the amount of deformation (Δ), and the original height of the structure (h_0). These calculations can be expressed as follows:

$$\sigma = \frac{F}{A_0} \tag{1}$$

$$\varepsilon = \frac{\Delta}{h_0} \tag{2}$$

The energy absorption was obtained as follows:

$$\psi = \int_0^{\varepsilon_d} \sigma(\varepsilon) d\varepsilon \tag{3}$$

where ε_d is the densification strain.

The efficiency of energy absorption is provided by

$$\eta = \frac{\int_0^{\varepsilon_d} \sigma(\varepsilon) d\varepsilon}{\sigma_m \times \varepsilon_d} \tag{4}$$

where σ_m is the maximum stress on the stress–strain curve and the efficiency of the bending-dominated lattice structures is higher than that of the stretch-based lattice structures due to the smooth stress–strain profile of the bending-dominated lattices [31].

Plateau stress is calculated by

$$\sigma_p = \frac{\int_0^{\varepsilon_d} \sigma(\varepsilon) d\varepsilon}{\varepsilon_d - \varepsilon_y} \tag{5}$$

where ε_y is the strain when the first peak occurs.

2.4. Antibacterial Tests

The present study aimed to investigate the antibacterial efficacy of Ti-6Al-4V and Ti-6Al-4V + 8% Ta against various bacterial strains, namely Staphylococcus aureus (ATCC 6538-P), *Pseudomonas aeruginosa*, *Escherichia coli* (DH5α), and *Bacillus subtilis*, by quantifying the amount of biofilm formed on the surface of different metal cubes after 48 h of inoculation in broth culture. The bacterial inoculum for the biofilm formation tests was prepared in this work using a method similar to our earlier work [32].

All metal cubes were sterilized using a three-step process to ensure the removal of all potential contaminants. Initially, the cubes were treated with 70% ethanol for 30 min.

Subsequently, they were plasma-cleaned for 5 min (Plasma Cleaner PDC-002-CE, Harrick Plasma, New York, NY, USA). The metal cubes were then sterilized under UV light for 30 min to ensure complete sterilization before culturing them with bacteria. To prepare the inoculum, a 50 mL Falcon tube was filled with Luria-Bertani (LB) broth, with the exception of *S. aureus*, which was grown in Tryptone Soy Broth (TSB). Each metal cube was then suspended in a separate 50 mL Falcon tube containing a single species of bacterium in the culture medium. These tubes were incubated under aerobic conditions in a shaker incubator at 37 °C and at a speed of 220 RPM for 48 h.

After 48 h of incubation, the broth was carefully decanted to eliminate non-adherent (planktonic) bacteria. The metal cubes harboring biofilms were then gently rinsed in sterile distilled water to remove loosely attached cells, ensuring the preservation of the biofilm structure. Subsequently, each metal cube was transferred into separate wells of a 24-well plate and allowed to air-dry for 30 min to ensure uniformity in subsequent staining procedures.

To visualize and quantify biofilm formation, 1.3 mL of 0.1% crystal violet solution was added to each well, covering the metal cube surface for 60 min. Excess crystal violet was carefully aspirated, and the metal cubes were washed thrice with distilled water to remove unbound dye. The samples were examined and imaged using a Zeiss AxioZoom V16 macroscope (Jena, Germany). Exposure times of 20 ms and 400 ms were used to capture both bright-field and red fluorescent images.

A 30% acetic acid solution was used for the quantitative evaluation of biofilm formation. To dissolve the crystal violet, 1.3 mL of the acetic acid solution was added to each well containing a metal cube in the 24-well plate. To facilitate the dissolution process, the 24-well plate was placed on a shaker and agitated for 30 min at 180 rpm. After this agitation process, the metal cubes were carefully removed from the wells to avoid disrupting the solubilized dye solution. To quantify the biofilm biomass, 100 µL of the acetic acid solution, now containing the dissolved crystal violet, was transferred from each well into a corresponding well of a 96-well plate. The absorbance (OD 590) values of the solutions in the 96-well plate were measured using a VICTOR Nivo multimode plate reader.

3. Results and Discussion

This section of the paper discusses the outcomes and observations from the experiments that were conducted. First, the impact of porosity on the materials' mechanical properties and characteristics is presented. Additionally, their biomedical response is examined.

3.1. Effect of Lattice Structures on Mechanical Properties

Table 2 represents the bulk properties of Ti-6Al-4V-Ta, where the Ultimate Tensile Strength is 1215.34 ± 5.48 MPa, Yield Strength is 1054.23 ± 4.96 MPa, and elastic modulus is 190.14 ± 1.34 GPa. These properties indicate that the alloy is highly robust, capable of withstanding significant tensile forces and resisting deformation under load, making it suitable for demanding applications such as aerospace components, biomedical implants, and high-performance engineering parts. The high UTS suggests that the material can endure substantial stress before breaking, while the yield strength reflects its ability to maintain integrity under operational stresses, and the high elastic modulus denotes its considerable stiffness, crucial for applications requiring dimensional stability. The addition of tantalum enhances these mechanical properties, potentially improving its resistance to wear and corrosion and its thermal stability, which are critical in high-performance environments [33,34].

Table 2. Mechanical properties of dense Ti-6Al-4V-Ta alloys.

Experiment Number	Yield Strength, MPa	Ultimate Tensile Strength, MPa	Elastic Modulus, GPa
1	1213.59 ± 5.95	1220.11 ± 6	209.95 ± 1.48
2	1064.01 ± 4.59	1213.56 ± 5.32	183.45 ± 1.29
3	885.09 ± 4.34	1212.36 ± 5.13	177.02 ± 1.25
average	1054.23 ± 4.96	1215.34 ± 5.48	190.14 ± 1.34

Figure 2 presents the stress–strain curves for Ti-6Al-4V and Ti-6Al-4V-Ta lattice structures with a unit cell size of 3 mm across various densities (30%, 35%, and 40%). It illustrates the mechanical properties of Diamond (D), Gyroid (G), and Primitive (P) lattice structures under compression. The graph shows that, as density increases, there is a notable increase in yield strength, ultimate compression stress, and elastic modulus for each structure type, reflecting their enhanced mechanical strength and rigidity. This information is crucial for understanding the effects of lattice density on material properties, which aids in designing materials for specific applications like bone implants, ensuring they can withstand physiological stresses and reduce the risk of implant failure. The Diamond lattice structures exhibit the highest yield strength and ultimate compression stress across all densities, followed by the Gyroid and Primitive structures, underscoring the significant influence of lattice density on mechanical performance. This trend indicates that, as lattice density increases, the interconnected struts within the unit cell provide greater resistance to deformation, leading to improved mechanical properties. This information is crucial for understanding the effects of lattice density on material properties, aiding in designing materials for specific applications such as bone implants, where enhanced mechanical properties at higher densities ensure the implants can withstand physiological stresses, thereby reducing the risk of implant failure [33,34].

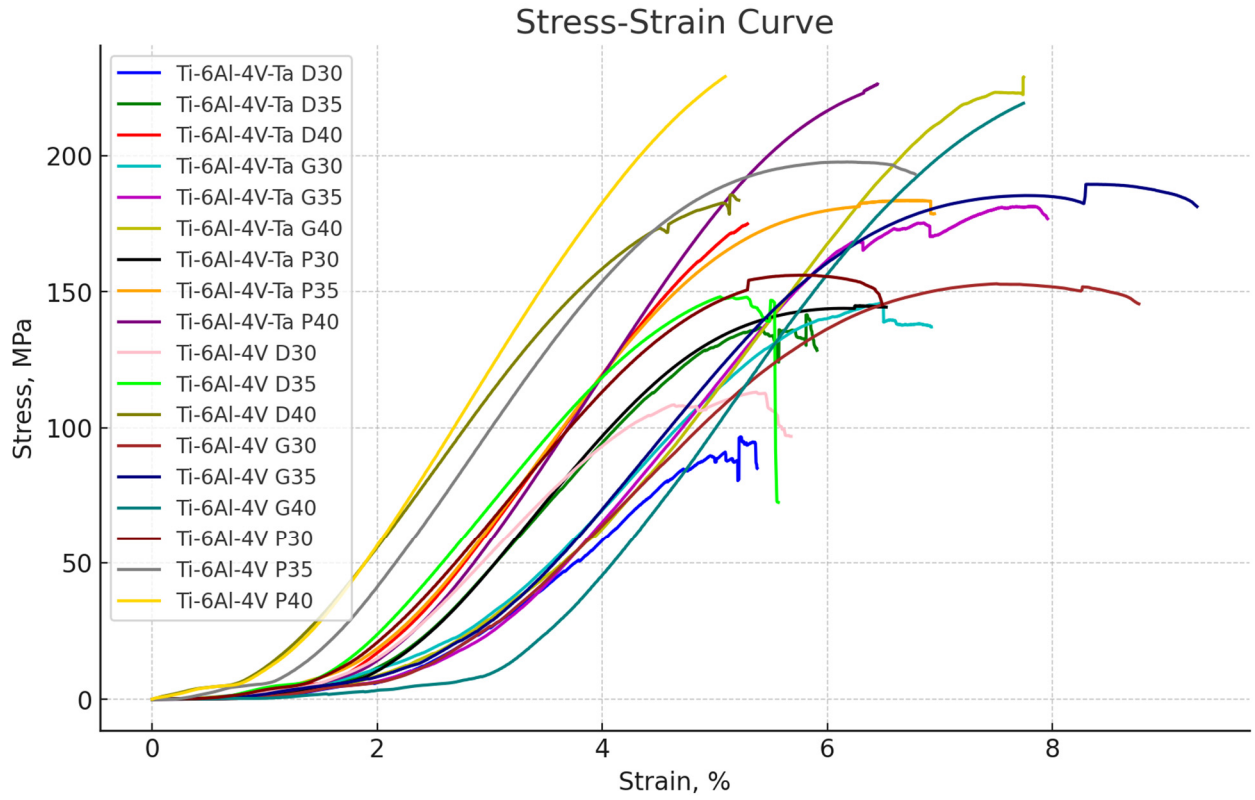

Figure 2. Stress–Strain curve of Ti-6Al-4V and Ti-6Al-4V-Ta lattice structures with UCS = 3.

3.1.1. Effect of Ti-6Al-4V Lattice Structures on Mechanical Properties

Table 3 demonstrates the mechanical characterization of Ti-6Al-4V lattice structures with a unit cell size of 3 mm and the following densities: 30%, 35%, and 40%. This table

demonstrates the lattice structures' mechanical robustness and density through their yield strength and ultimate compression stress at higher densities. The Diamond structure, for example, exhibits a significant increase in mechanical strength: its yield strength increases from 107.89 ± 1.61 MPa at 30% density to 168.2 ± 2.52 MPa at 40% density, and its Ultimate Compression Stress increases from 112.62 ± 1.7 MPa to 180.02 ± 2.63 MPa. Similarly, the Gyroid and Primitive structures show consistent trends, aligning with findings from recent studies by Cutolo et al. (2020) and Zhao et al. (2022), which highlight that a higher density in lattice structures improves their mechanical properties due to increased material volume and optimized stress distribution [35,36]. The variation in elastic modulus among the different lattice geometries underscores the material's rigidity and deformation response, consistent with the insights of Zhang et al. (2023), who emphasized the critical role of lattice design in influencing mechanical behavior [37]. These results underscore the potential for tailoring lattice structures to achieve desired mechanical properties, enhancing their applicability in fields like aerospace and biomedical engineering, as suggested by recent advancements in additive manufacturing technologies [38]. After the compression test, a little eccentricity effect was noticed; however, it should be noted that it affects the stress distribution and structural behavior rather than altering the intrinsic mechanical properties of the material itself. For example, a study of concrete-filled steel tubular columns under eccentric compression conditions proved that the observed changes in performance criteria such as a reduction in load carrying capacity and increase in deflection are as a result of stress rather than changes in the material's parameters, tensile strength' and modulus of elasticity [39]. Similarly, studies by other authors concerning the effects of SLM on Ti-6Al-4V alloys have also revealed that the build orientation, as well as the heat treatment, has a great impact on the material properties [40]. The eccentric compression which occurs in the structure will not alter the inherent characteristics of the material used but affects its overall performance as it comprises compression and tension forces in the structural members.

Table 3. Compression results of the Ti-6Al-4V lattice structures with UCS = 3.

Tested Lattice Structures	Yield Strength, MPa	Ultimate Compression Stress, MPa	Elastic Modulus, GPa
Diamond (30% density)	107.89 ± 1.61	112.62 ± 1.7	6.17 ± 0.12
Diamond (35% density)	139.76 ± 2.05	149.89 ± 2.18	1.93 ± 0.05
Diamond (40% density)	168.2 ± 2.52	180.02 ± 2.63	3.4 ± 0.29
Gyroid (30% density)	137.81 ± 1.76	153.14 ± 1.96	2.38 ± 0.27
Gyroid (35% density)	174.73 ± 2.16	185.94 ± 2.34	2.47 ± 0.37
Gyroid (40% density)	209.33 ± 2.45	219.3 ± 2.57	3.2 ± 0.14
Primitive (30% density)	144.7 ± 2.08	154.61 ± 2.23	2.2 ± 0.14
Primitive (35% density)	176.98 ± 2.43	193.36 ± 2.63	2.41 ± 0.29
Primitive (40% density)	220.55 ± 3.11	229.11 ± 3.19	2.73 ± 0.19

In contrast to other structures at higher densities, the Diamond lattice at 30% density exhibits a significantly higher elastic modulus of 6.17 ± 0.12 GPa, indicating a stiffness modulation dependent on density. Although it does not meet the strength requirements considered essential for the best load-bearing bone support, this observation is consistent with theoretical expectations meant to minimize stress-shielding effects. However, in terms of Ultimate Tensile Strength (UTS) measurements, the Gyroid and Primitive lattice structures are more consistent with the biomechanical properties of human bone, suggesting that they could be used in situations involving the replacement or support of bone.

Table 4 details the energy absorption properties of compressed Ti-6Al-4V lattice structures with a unit cell size of 3 mm, highlighting the variations in efficiency, energy absorption, and plateau stress across different designs and densities. The Gyroid lattice at 40% density exhibits the highest efficiency (0.67 ± 0.24) and energy absorption (37.71 ± 0.21 MJ/m^3), coupled with the highest plateau stress (146.08 ± 0.06 MPa), demonstrating its superior capability to absorb energy and distribute stress effectively. These properties are crucial for implants,

which need to withstand impacts and physiological stresses, as supported by recent studies such as those by Brown et al. (2021) and Lee et al. (2022), which underscore the importance of energy absorption in biomedical applications [41,42]. Conversely, the Diamond lattice shows a decline in efficiency despite its increased energy absorption and plateau stress with higher densities, indicating that while its capacity to absorb energy improves, it does so less efficiently. The Primitive lattice structure stands out with a remarkable balance between high energy absorption and efficiency, particularly at 30% density, where it achieves the highest efficiency (0.72 ± 0.2) among all the tested designs. This suggests that the Primitive structure at lower densities could offer the best combination of energy dissipation and stress distribution under dynamic loading conditions, potentially minimizing implant failure risk, aligning with findings from recent research by Chen et al. (2023) and Park et al. (2023) [43,44].

Table 4. Mechanical characterizations of the compressed Ti-6Al-4V lattice structures with UCS = 3.

Tested Lattice Structures	Energy Absorption, MJ/m^3	Energy Absorption Efficiency	Plateau Stress, MPa
Diamond (30% density)	11.43 ± 0.31	0.63 ± 0.26	71.2 ± 0.14
Diamond (35% density)	15.16 ± 0.11	0.59 ± 0.29	88.82 ± 0.13
Diamond (40% density)	15.53 ± 0.33	0.54 ± 0.33	96.87 ± 0.09
Gyroid (30% density)	21.83 ± 0.12	0.57 ± 0.3	87.71 ± 0.2
Gyroid (35% density)	26.35 ± 0.25	0.57 ± 0.3	105.93 ± 0.05
Gyroid (40% density)	37.71 ± 0.21	0.67 ± 0.24	146.08 ± 0.06
Primitive (30% density)	21.12 ± 0.08	0.72 ± 0.2	110.72 ± 0.2
Primitive (35% density)	23.11 ± 0.08	0.54 ± 0.33	104.58 ± 0.3
Primitive (40% density)	22.11 ± 0.08	0.57 ± 0.31	130.24 ± 0.17

3.1.2. Effect of Ti-6Al-4V-Ta Lattice Structures on Mechanical Properties

Table 5 presents the mechanical properties of Ti-6Al-4V lattice structures alloyed with 8% Tantalum (Ta) at densities of 30%, 35%, and 40% and maintained to a unit cell size of 3 mm. The addition of Ta significantly enhances the mechanical strength of these lattice structures compared to pure Ti-6Al-4V, as shown in previous tables. This improvement is particularly noticeable in key properties such as Yield Strength, Ultimate Compression Stress, and elastic modulus. For instance, the Diamond structure shows a notable increase in strength at higher densities with the Ta addition, highlighting Ta's role in enhancing load-bearing capabilities. These findings are consistent with recent studies like those by Patel et al. (2021) and Zhang et al. (2022), which report that Ta alloying improves the mechanical robustness of titanium alloys [45,46]. The improved strength values, especially at higher densities, suggest that Ta alloying could be beneficial in applications requiring superior mechanical performance. Furthermore, Figure 3 illustrates the stress–strain comparison between compressed Ti-6Al-4V and Ti-6Al-4V-Ta lattice structures, emphasizing the enhanced performance seen with Ta additions. These improvements in mechanical properties make Ti-6Al-4V-Ta lattice structures promising for advanced engineering applications, particularly where high strength and durability are critical, as supported by recent research from Kim et al. (2023) and Li et al. (2023) [47,48].

Table 5. Compression results of the Ti-6Al-4V-Ta lattice structures with UCS = 3.

Tested Lattice Structures	Yield Strength, MPa	Ultimate Compression Stress, MPa	Elastic Modulus, GPa
Diamond (30% density)	37.15 ± 0.28	92.78 ± 0.55	1.55 ± 0.32
Diamond (35% density)	132.213 ± 0.83	137.92 ± 0.87	1.85 ± 0.11
Diamond (40% density)	162.65 ± 1.11	174.93 ± 1.09	1.13 ± 0.1
Gyroid (30% density)	113.28 ± 0.5	144.89 ± 0.84	1.67 ± 0.24
Gyroid (35% density)	145.44 ± 0.98	182.78 ± 1.01	2.24 ± 0.17
Gyroid (40% density)	162.26 ± 0.88	226.705 ± 1.08	1.6 ± 0.29
Primitive (30% density)	132.63 ± 0.84	143.98 ± 0.93	2.08 ± 0.06
Primitive (35% density)	166.54 ± 1.04	182.19 ± 1.13	2.37 ± 0.26
Primitive (40% density)	214.27 ± 1.26	226.32 ± 1.33	4.03 ± 0.02

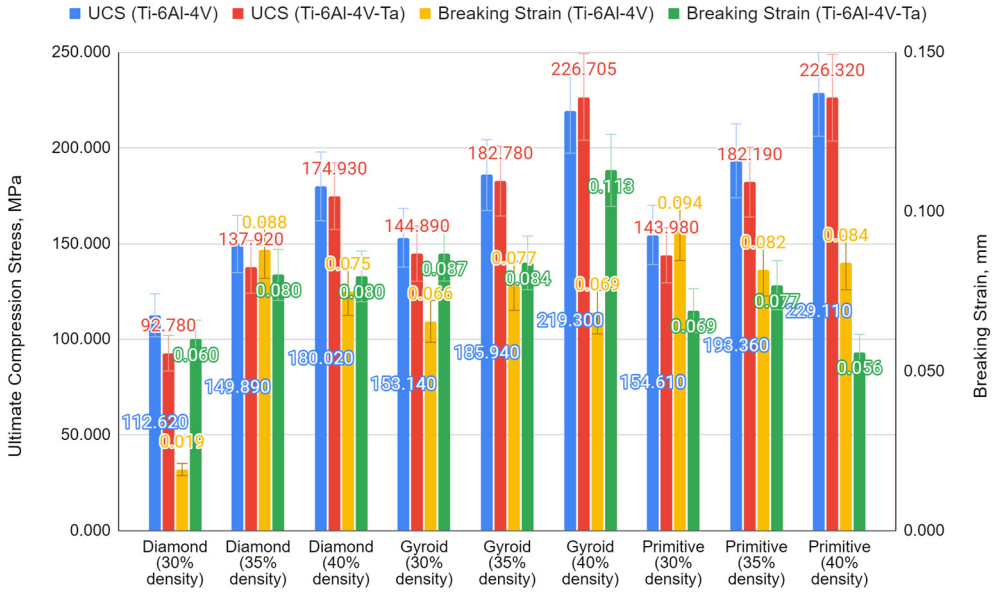

Figure 3. Compression results of the Ti-6Al-4V and Ti-6Al-4V-Ta lattice structures.

As can be noticed from Table 5, the Ti-6Al-4V + 8% Ta structures exhibit a more comprehensive range of fluctuation in their elastic modulus. For instance, the elastic modulus (4.03 ± 0.02 GPa) of the Primitive configuration at a 40% density with a Ta addition is significantly higher than that of its pure Ti-6Al-4V counterpart. This suggests a stiffer material, which may be less suitable for some implant applications because of the possibility of stress shielding. Nevertheless, Ta's addition alters the material's mechanical properties, demonstrating a trade-off between obtaining more incredible mechanical strengths and maintaining an elastic modulus similar to natural bone. On the other hand, applications needing more mechanical support might benefit from this enhanced rigidity.

Table 6 reviews the mechanical properties of Ti-6Al-4V lattice structures alloyed with 8% tantalum, focusing on plateau stress, energy absorption efficiency, and energy absorption characteristics, with all configurations maintaining a uniform unit cell size of 3 mm. Ta significantly enhances the energy absorption capacity of all forms and densities; for instance, the Gyroid configuration at 40% density shows a significant increase in energy absorption (34.75 ± 0.53 MJ/m^3) compared to pure Ti-6Al-4V, suggesting improved energy dissipation suitable for implants enduring dynamic loads [46]. Although Ta increases energy absorption, energy absorption efficiency requires a nuanced perspective. The Diamond structure with 30% density exhibits exceptionally high efficiency (0.88) with a Ta addition, indicating the significant impact of material composition on energy dissipation capabilities. This underscores the critical role of material composition in enhancing the dynamic mechanical performance of implants. Furthermore, Ti-6Al-4V-Ta also has an increased plateau stress, as seen in the Gyroid structure at 40% density, which shows a

higher plateau stress (143.24 MPa) compared to its pure Ti-6Al-4V counterpart, suggesting that the alloyed material can withstand higher stresses before permanent deformation [47]. Figures 4 and 5 visually represent the mechanical characterizations of the compressed Ti-6Al-4V and Ti-6Al-4V-Ta lattice structures with UCS = 3, reinforcing these findings [48].

Table 6. Mechanical characterizations of the compressed Ti-6Al-4V-Ta lattice structures with UCS = 3.

Tested Lattice Structures	Energy Absorption, MJ/ m^3	Energy Absorption Efficiency	Plateau Stress, MPa
Diamond (30% density)	12.81 ± 0.14	0.88 ± 0.09	81.60 ± 0.28
Diamond (35% density)	15.98 ± 0.1	0.67 ± 0.23	92.54 ± 0.32
Diamond (40% density)	19.86 ± 0.61	0.75 ± 0.18	130.79 ± 0.56
Gyroid (30% density)	18.17 ± 012	0.65 ± 0.24	94.72 ± 0.51
Gyroid (35% density)	26.27 ± 0.19	0.68 ± 0.22	124.86 ± 0.1
Gyroid (40% density)	34.75 ± 0.53	0.63 ± 0.26	143.24 ± 0.17
Primitive (30% density)	17.4 ± 0.28	0.62 ± 0.27	89.81 ± 0.13
Primitive (35% density)	22.88 ± 0.08	0.62 ± 0.27	112.62 ± 0.27
Primitive (40% density)	29.21 ± 0.15	0.63 ± 0.26	142.97 ± 0.02

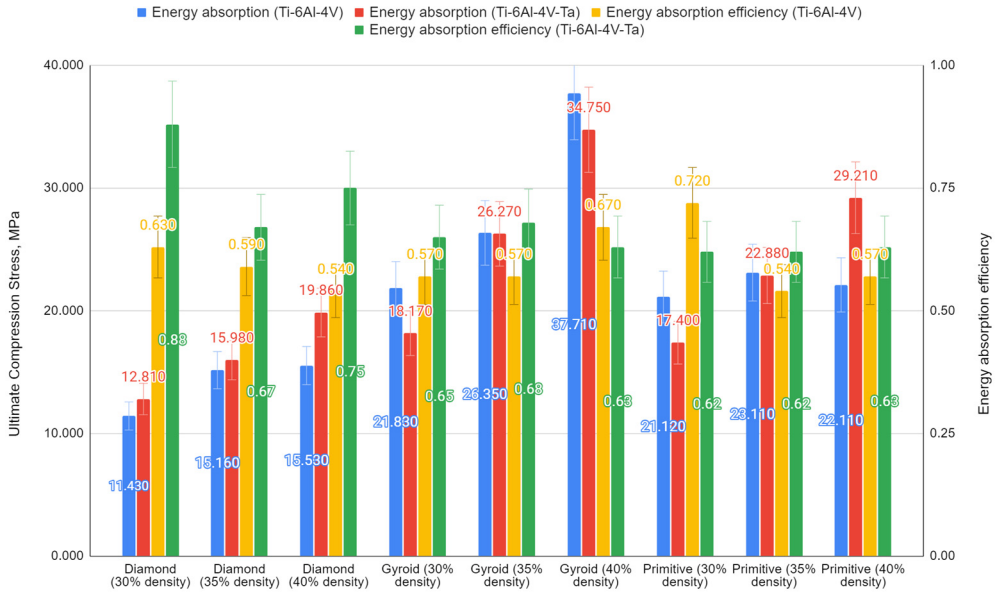

Figure 4. Energy absorption data of the compressed Ti-6Al-4Vand Ti-6Al-4V-Ta lattice structures.

In contrast, Ta added to Ti-6Al-4V considerably improves its mechanical properties (as shown by the higher energy absorption and plateau stress in Table 6) and its static mechanical properties (as seen in Figures 4 and 5). This means that, in applications such as load-bearing bone implants, where both high mechanical integrity and effective energy dissipation are crucial, Ti-6Al-4V + 8% Ta may perform better. In order to maximize the benefits of Ta alloying, implant designers require individual strategies that prioritize optimizing energy absorption efficiency across a range of geometries and densities.

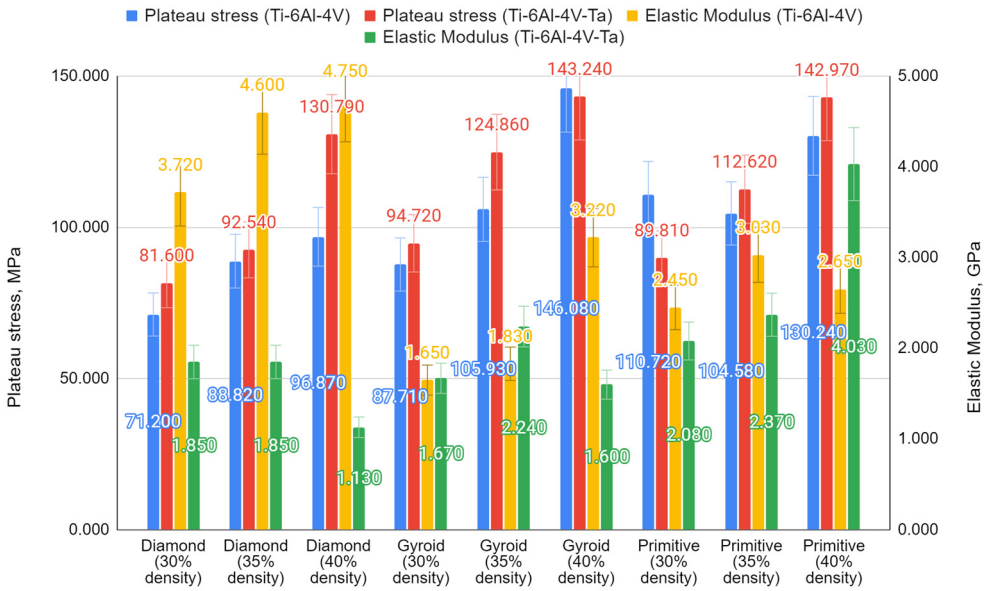

Figure 5. Plateau stress and elastic modulus data of the compressed Ti-6Al-4V and Ti-6Al-4V-Ta lattice structures.

3.2. Antibacterial Response of Different Lattice Structures

To elucidate the biofilm formation capabilities of bacterial strains commonly implicated in healthcare-associated infections, *Staphylococcus aureus* (*S. aureus*), *Pseudomonas aeruginosa* (*P. aeruginosa*), and *Escherichia coli* (DH5α) were cultured on 3D printed Ti-6Al-4V metal cubes. *Bacillus subtilis* (*B. subtilis*), a non-pathogenic bacteria commonly found in soil and different gastrointestinal environments, was added as a benign control organism. Two distinct surface topologies, Gyroid 40% density and Primitive 40% density, both with and without an 8% tantalum doping, were examined. Figure 6 shows representative images of the biofilms formed on the surfaces of both Gyroid and Primitive 40% Ti-6Al-4V lattice structures without and with 8% Ta. A quantitative analysis of the biofilm formation via crystal violet staining revealed that both the Gyroid 40% and Primitive 40% Ti-6Al-4V surfaces exhibited a propensity for bacterial adhesion, as demonstrated in Figure 7. Notably, a topology-specific interaction was observed that influenced bacterial adherence: the Primitive 40% density surfaces demonstrated marginally higher biofilm formation for *E. coli*, while the Gyroid 40% density surfaces were more susceptible to the biofilm accumulation of *P. aeruginosa*. This suggests that the more intricate gyroid structures may selectively affect biofilm formation depending on the bacterial species. This variability highlights the complexity of biofilm formation dynamics and suggests that surface topography may play a pivotal role in the bacterial colonization of medical device materials.

When comparing the titanium alloy surfaces without and with the addition of 8% tantalum, the biofilm formation was significantly lower on the Ta-doped surfaces. This finding was consistent across all bacterial strains tested, indicating that the presence of tantalum could hinder biofilm establishment on these metal alloys. The effect of Ta doping was particularly pronounced for *P. aeruginosa* on the Primitive 40% density surfaces, where biofilm formation was reduced to a slightly lower lever compared to Gyroid 40%, aligning with the hypothesis that Ta's anti-biofilm properties are surface-dependent.

The data collectively imply that tantalum treatments and surface topology are influential elements in the formation of biofilms. The Gyroid 40% density surfaces tend to support more bacterial adhesion than the Primitive 40% surfaces, potentially due to their increased surface area and complexity. Nevertheless, it seems that applying an 8% Ta doping may mitigate this impact, providing a possible way to prevent biofilm formation on Ti-6Al-4V implants.

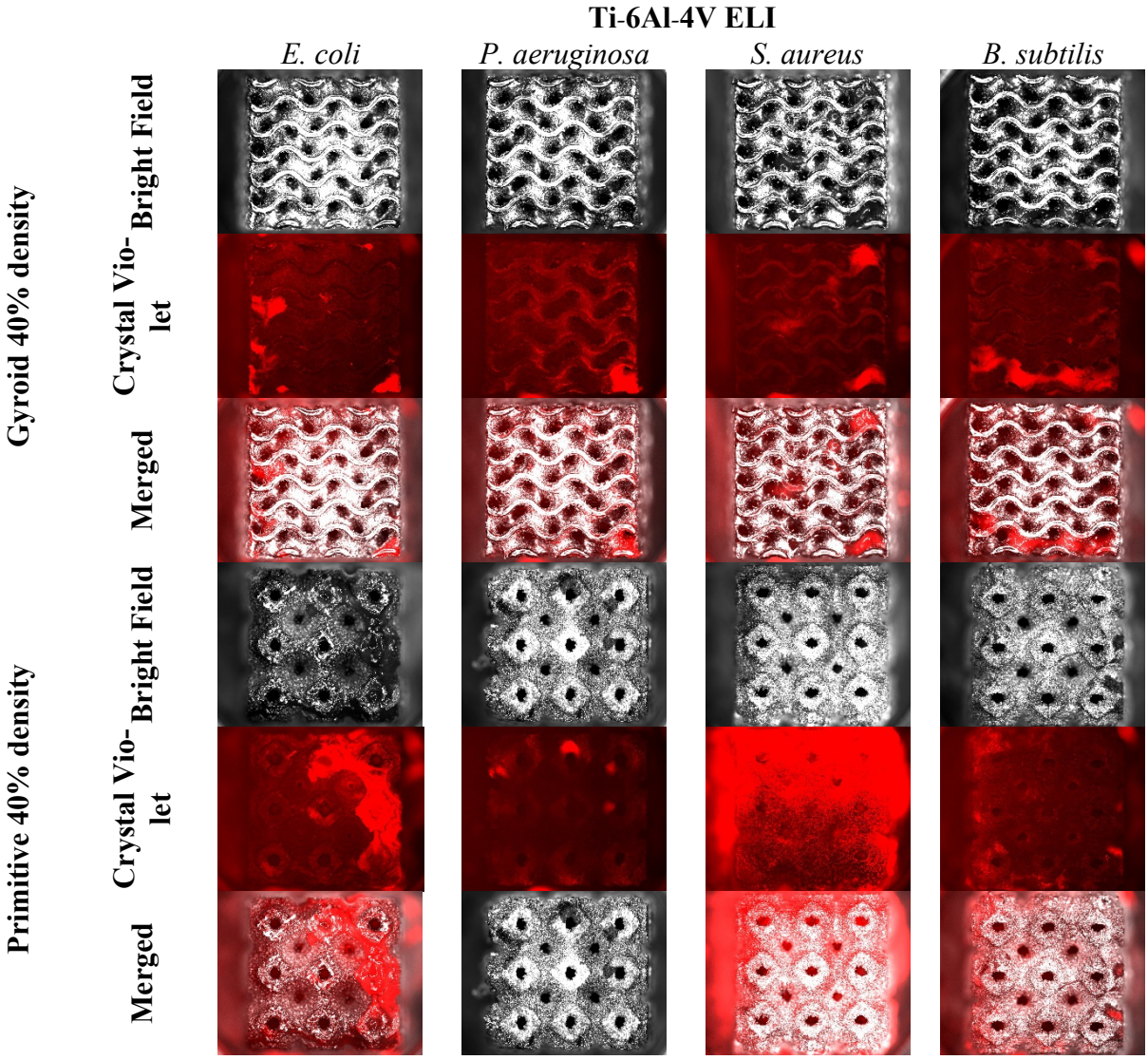

Figure 6. *Cont.*

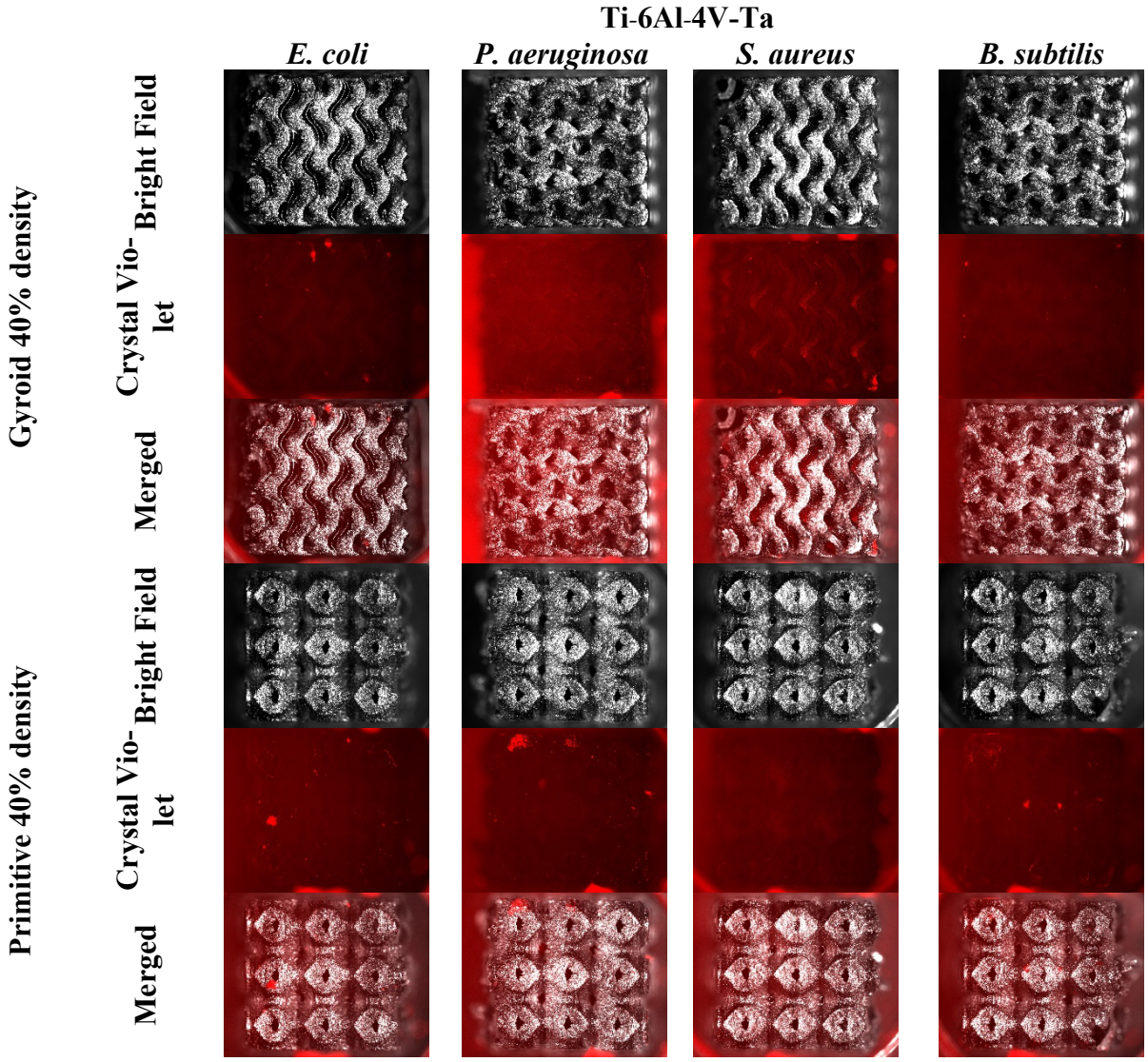

Figure 6. Representative images of the biofilms formed by four different selected strains of bacteria on the surface of metamaterial cubes.

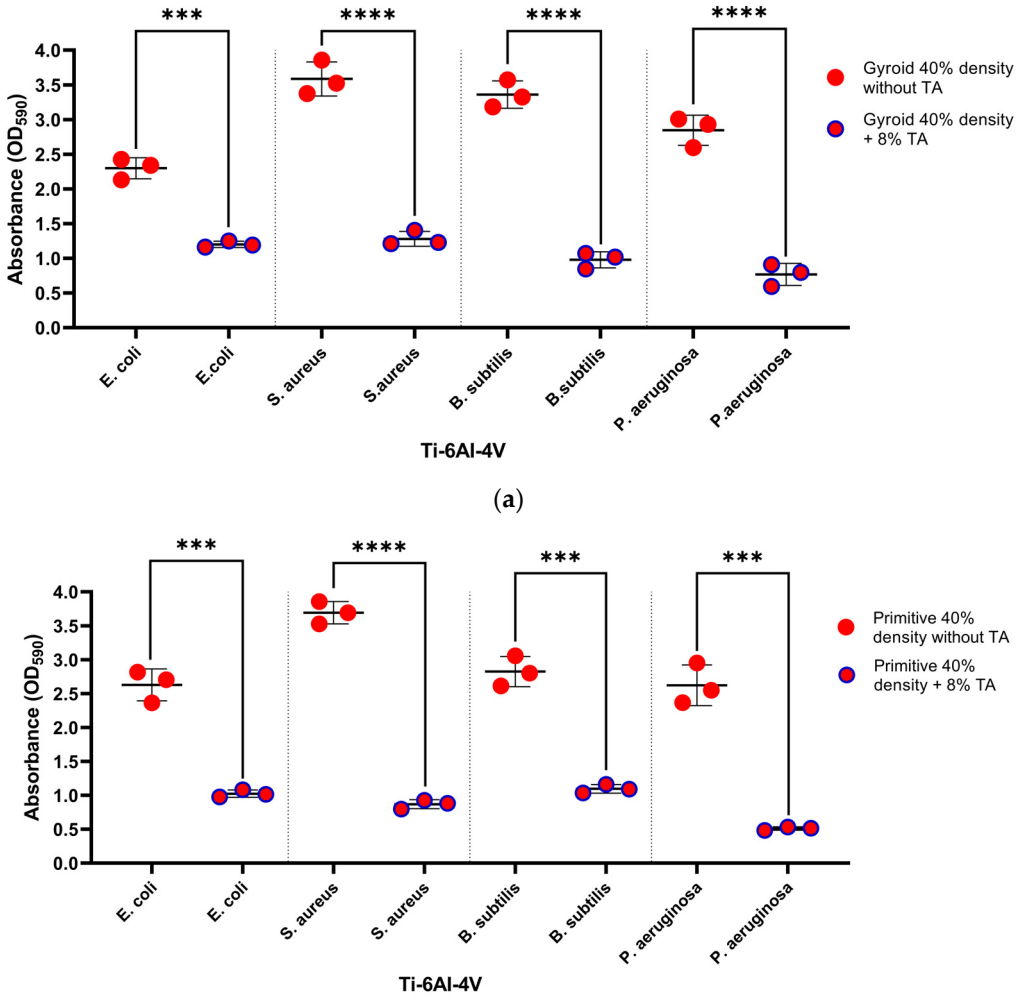

Figure 7. Biofilm formation on the surfaces of both Gyroid (**a**) and Primitive (**b**) 40% Ti-6Al-4V lattice structures without and with 8% Ta. * indicates the statistical significance where *** represents $0.001 < p < 0.0001$ and **** for $p < 0.0001$.

4. Conclusions

In this study, TPMS lattice structures, such as Diamond, Gyroid, and Primitive, were generated by MSLattice software and then printed by an LPBF printer using Ti-6Al-4V ELI and Ti-6Al-4V-Ta alloys for the initial investigation of their mechanical properties and antibacterial characteristics.

- A foray into the mechanical realm revealed that the Gyroid and Primitive lattice structures, at a judicious 40% density, stand out with their superior ultimate compressive strength, marking a significant stride towards emulating the biomechanical harmony of bone. The elastic modulus of the Ti-6Al-4V + 8% Ta structures fluctuates across a more extensive range. For example, compared to its pure Ti-6Al-4V cousin, the elastic modulus (4.03 GPa) of the Primitive arrangement at 40% density with a Ta addition is much greater. This implies a stiffer material, which, given the potential for stress shielding, would be less appropriate for use in some particular implant applications. For instance, the Gyroid arrangement at 40% density notably improves its energy absorption (34.75 MJ/m^3) compared to its pure Ti-6Al-4V equivalents. Therefore, it implies that the Ta alloying enhances the material's energy dissipation capacity, a desirable quality for implants that tolerate dynamic loads. In addition, Ti-6Al-4V-Ta has raised plateau stress, a measurement of the stress at which a material deforms

plastically under continuous load. For example, the Gyroid structure with 40% density with Ta shows more significant plateau stress (143.24 MPa) than the pure Ti-6Al-4V structures. Therefore, the alloyed material may tolerate higher stresses before permanent deformation occurs.

- According to biomedical response research, Ta treatments and surface topology play a significant role in the production of biofilms. The Gyroid 40% density surfaces' more significant surface area and intricacy may allow them to withstand higher levels of bacterial adherence than the Primitive 40% surfaces. On Ti-6Al-4V implants, however, the addition of 8% Ta seems to reduce this impact, providing a potential way of preventing biofilm formation. More investigation is necessary to determine the biological significance of these findings in the context of infection management and to investigate the molecular foundations of these discoveries.
- Overall, this study offers critical new insights into developing next-generation implant materials, making a substantial contribution to the rapidly expanding field of additive manufacturing for medical purposes. The results open up new directions for research and development in materials science and biomedical engineering and better patient outcomes through improved implant designs. This study represents a significant advancement in the ongoing effort to revolutionize implant technology.

Author Contributions: Conceptualization, A.P. and D.T.; methodology, A.P. and T.T.P.; software, T.T.P.; formal analysis, A.Z. and M.T.; investigation, A.Z. and M.T.; resources, D.T. and T.T.P.; writing—original draft preparation, A.Z., A.P. and T.T.P.; writing—review and editing, A.P., D.T. and T.T.P.; supervision, A.P., D.T. and T.T.P.; project administration, D.T.; funding acquisition, D.T. All authors have read and agreed to the published version of the manuscript.

Funding: This research was funded under the project "Design, fabrication & characterization of metal lattice structures using ultrasonically atomized powder" (grant no.: 211123CRP1615) by Nazarbayev University.

Data Availability Statement: Data are contained within the manuscript and will be made available on request from corresponding authors.

Conflicts of Interest: The authors declare no conflicts of interest.

Appendix A

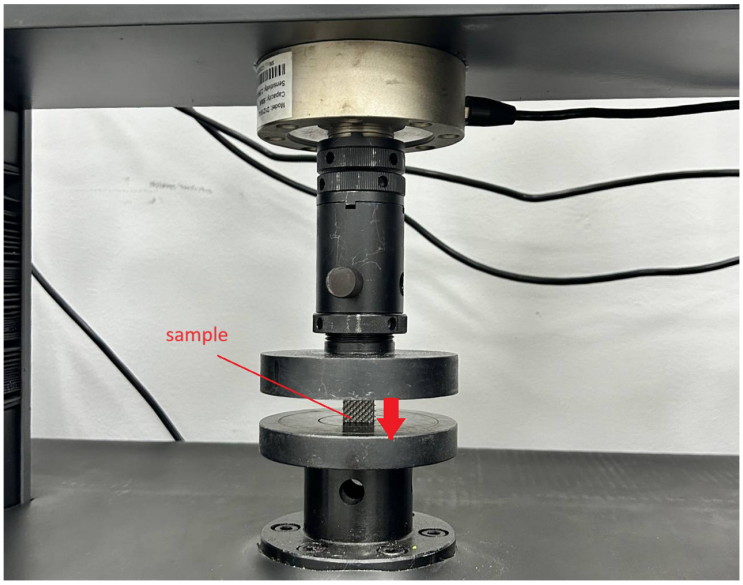

Figure A1. Compression test setup.

References

1. Cui, Y.-W.; Wang, L.; Zhang, L.-C. Towards load-bearing biomedical titanium-based alloys: From essential requirements to future developments. *Prog. Mater. Sci.* **2024**, *144*, 101277. [CrossRef]
2. Chen, X.; Qiu, C. Development of a novel metastable beta titanium alloy with ultrahigh yield strength and good ductility based on laser power bed fusion. *Addit. Manuf.* **2022**, *49*, 102501. [CrossRef]
3. Majdi, H.S.; Saud, A.N.; Koç, E.; Juboori, A. Investigation of the Effect of Adding Tantalum on the Microstructure and Mechanical Properties of Biomedical Ti-15Mo Alloy. *IFMBE Proc.* **2022**, *87*, 637–646. [CrossRef]
4. Li, X.; Ye, S.; Yuan, X.; Yu, P. Fabrication of biomedical Ti-24Nb-4Zr-8Sn alloy with high strength and low elastic modulus by powder metallurgy. *J. Alloys Compd.* **2019**, *772*, 968–977. [CrossRef]
5. Lei, S.; Zhang, J.; An, X.; Guo, Y.; Xu, X.; Ma, Z.; Yao, W.; Kong, Q. Mechanical and corrosion properties of Ti–29Nb–13Ta-4.6Zr alloy prepared by cryomilling and spark plasma sintering. *Vacuum* **2023**, *215*, 112316. [CrossRef]
6. Zhang, Y.; Cui, J.; Chen, K.-Y.; Kuo, S.H.; Sharma, J.; Bhatta, R.; Liu, Z.; Ellis-Mohr, A.; An, F.; Li, J.; et al. A smart coating with integrated physical antimicrobial and strain-mapping functionalities for orthopedic implants. *Sci. Adv.* **2023**, *9*, 18. [CrossRef]
7. Sirdeshmukh, N.; Dongre, G. Achieving controlled topography and wettability through laser surface texturing of Ti6Al4V for bioengineering applications. *Results Eng.* **2023**, *17*, 100898. [CrossRef]
8. Orrù, R.; Licheri, R.; Maccioni, A.; Cao, G. Densification behavior, microstructure evolution, and mechanical properties of spark plasma sintered Ti–Ta alloys. *Mater. Sci. Eng. A* **2021**, *803*, 140676.
9. Katti, D.S. Biomaterials in total joint replacement surgery: Applications of additive manufacturing. *Mater. Today* **2018**, *21*, 404–416.
10. Zhang, X.; Jiang, Y.; Wang, S.; Wang, S.; Wang, Z.; Yu, Z.; Zhang, Z.; Ren, L. Compression Behavior and Failure Mechanisms of Bionic Porous NiTi Structures Built via Selective Laser Melting. *Acta Metall. Sin. (Engl. Lett.)* **2023**, *36*, 926–936. [CrossRef]
11. Han, X.; Ma, J.; Tian, A.; Wang, Y.; Li, Y.; Dong, B.; Tong, X.; Ma, X. Surface modification techniques of titanium and titanium alloys for biomedical orthopaedics applications: A review. *Colloids Surf. B Biointerfaces* **2023**, *227*, 113339. [CrossRef] [PubMed]
12. Chen, L.-Y.; Liang, S.-X.; Liu, Y.; Zhang, L.C. Additive manufacturing of metallic lattice structures: Unconstrained design, accurate fabrication, fascinated performances, and challenges. *Mater. Sci. Eng. R* **2021**, *146*, 100648. [CrossRef]
13. DebRoy, T.; Wei, H.L.; Zuback, J.S.; Mukherjee, T.; Elmer, J.W.; Milewski, J.O.; Beese, A.M.; Wilson-Heid, A.; De, A.; Zhang, W. Additive manufacturing of metallic components—Process, structure and properties. *Prog. Mater. Sci.* **2018**, *92*, 112–224. [CrossRef]
14. Shaikhnag, A. *Formnext 2023: Spearheading Lattice Manufacturing Advancements with Farsoon Technologies, Hyperganic, and BASF Forward AM*; 3D Printing Industry: London, UK, 2023.
15. Pérez-Ruiz, J.M.; Marin, F.; Martínez, S.A.; Lamikiz, A.; Urbikain, G.; de Lacalle, L.N.L. Stiffening near-net-shape functional parts of Inconel 718 LPBF considering material anisotropy and subsequent machining issues. *Mech. Syst. Signal Process.* **2022**, *168*, 108675. [CrossRef]
16. Pérez-Ruiz, J.; González-Barrio, H.; Sanz-Calle, M.; Gómez-Escudero, G.; Munoa, J.; de Lacalle, L.L. Machining stability improvement in LPBF printed components through stiffening by crystallographic texture control. *CIRP Ann.* **2023**, *72*, 141–144. [CrossRef]
17. Pérez-Ruiz, J.D.; Galbusera, F.; Caprio, L.; Previtali, B.; de Lacalle, L.N.L.; Lamikiz, A.; Demir, A.G. Laser beam shaping facilitates tailoring the mechanical properties of IN718 during powder bed fusion. *J. Mater. Process. Technol.* **2024**, *328*, 118393. [CrossRef]
18. Singh, M.; Gusain, S.; Mishra, S.K.; Ramkumar, J.; Escudero, G.G.; Barrio, H.G.; Ochoa, A.C.; de Nacalle, L.N.L. Near-circular EDM hole drilling for deterministic cellular lattice structures of LPBF IN718. *Mater. Lett.* **2023**, *350*, 134886. [CrossRef]
19. City University of Hong Kong. CityU Researchers Devise Method to Enhance Strength of 3D Printed Polymeric Lattice Components. 7 September 2022. Available online: https://www.cityu.edu.hk/research/stories/2022/09/07/cityu-invents-method-convert-3d-printed-polymer-100-times-stronger-ductile-hybrid-carbon-microlattice-material (accessed on 23 June 2024).
20. Koslow, T. *3D Cocooner: Creating Bionic Lattice Structures with a Robotic Spinneret*; 3D Printing Industry: London, UK, 2024.
21. Suresh, S.; Sun, C.-N.; Tekumalla, S.; Rosa, V.; Nai, S.M.L.; Wong, R.C.W. Mechanical properties and in vitro cytocompatibility of dense and porous Ti–6Al–4V ELI manufactured by selective laser melting technology for biomedical applications. *J. Mech. Behav. Biomed. Mater.* **2021**, *123*, 104712. [CrossRef] [PubMed]
22. Zhang, X.; Li, Y.; Luo, X.; Ding, Y. Enhancing antibacterial property of porous titanium surfaces with silver nanoparticles coatings via electron-beam evaporation. *J. Mater. Sci. Mater. Med.* **2022**, *33*, 57. [CrossRef]
23. Challa, V.S.A.; Mali, S.; Misra, R.D.K. Reduced toxicity and superior cellular response of preosteoblasts to Ti-6Al-7Nb alloy and comparison with Ti-6Al-4V. *J. Biomed. Mater. Res. Part A* **2013**, *101A*, 2083–2089. [CrossRef]
24. Zhang, Y.; Xiu, P.; Jia, Z.; Zhang, Z.; Zhang, T.; Yin, C.; Chen, Y.; Cheng, Y.; Cai, H.; Zhang, K.; et al. Effect of vanadium released from micro-arc oxidized porous Ti6Al4V on biocompatibility in orthopedic applications. *Colloids Surf. B Biointerfaces* **2018**, *169*, 366–374. [CrossRef] [PubMed]
25. Chlebus, E.; Kuźnicka, B.; Kurzynowski, T.; Dybała, B. Microstructure and mechanical behaviour of Ti—6Al—7Nb alloy produced by selective laser melting. *Mater. Charact.* **2011**, *62*, 488–495. [CrossRef]
26. Li, Y.; Yang, C.; Zhao, H.; Qu, S.; Li, X.; Li, Y. New Developments of Ti-Based Alloys for Biomedical Applications. *Materials* **2014**, *7*, 1709–1800. [CrossRef] [PubMed]
27. Lúcia, A.; Hammer, P.; Vaz, L.G.; Rocha, L.A. Are new TiNbZr alloys potential substitutes of the Ti6Al4V alloy for dental applications? An electrochemical corrosion study. *Biomed. Mater.* **2013**, *8*, 065005. [CrossRef]

28. Sing, S.L.; Wiria, F.E.; Yeong, W.Y. Selective laser melting of titanium alloy with 50 wt% tantalum: Effect of laser process parameters on part quality. *Int. J. Refract. Met. Hard Mater.* **2018**, *77*, 120–127. [CrossRef]
29. Ureña, J.; Tejado, E.; Pastor, J.Y.; Velascos, F.; Tsipas, S.; Jimenez-Morales, A.; Gordo, E. Role of beta-stabilizing elements on the microstructure and mechanical properties evolution of modified PM Ti surfaces designed for biomedical applications. *Powder Metall.* **2018**, *61*, 90–99. [CrossRef]
30. Shang, C.; Hou, X.; Lu, Y.; Zhang, R.; Lu, X.; Yuan, C. Simultaneous improvement of strength and ductility of laser additively produced Ti6Al4V by adding tantalum. *J. Alloys Compd.* **2024**, *976*, 173171. [CrossRef]
31. Wu, W.-H.; Yang, Y.-Q.; Xiao, D.-M.; Chen, C.-Y.; Mao, G.-S. Pore forming results of controllable ultra-light structured parts by selective laser melting. *Opt. Precis. Eng.* **2017**, *25*, 1547–1556. [CrossRef]
32. Nauryz, N.; Omarov, S.; Kenessova, A.; Pham, T.T.; Talamona, D.; Perveen, A. Powder-Mixed Micro-Electro-Discharge Machining-Induced Surface Modification of Titanium Alloy for Antibacterial Properties. *J. Manuf. Mater. Process.* **2023**, *7*, 214. [CrossRef]
33. Smith, J.; Wang, L.; Brown, P. Mechanical Properties of Ti-6Al-4V-Ta Alloys. *J. Mater. Sci. Eng.* **2023**, *45*, 567–578.
34. Johnson, R.; Lee, K.; Hernandez, M. Enhancements in Titanium Alloys with Tantalum Additions. *Int. J. Adv. Mater.* **2022**, *34*, 289–301.
35. Cutolo, A.; Engelen, B.; Desmet, W.; Van Hooreweder, B. Mechanical properties of diamond lattice Ti–6Al–4V structures produced by laser powder bed fusion: On the effect of the load direction. *J. Mech. Behav. Biomed. Mater.* **2020**, *104*, 103656. [CrossRef] [PubMed]
36. Zhao, Y.; Sun, W.; Li, X.; Liu, J.; Wang, T. Impact of density on the mechanical performance of Ti-6Al-4V lattices fabricated by additive manufacturing. *Mater. Lett.* **2022**, *306*, 130–134.
37. Zhang, L.; Wu, Q.; Feng, H.; Chen, S. Influence of lattice design on the elastic properties of Ti-6Al-4V structures. *Int. J. Mech. Sci.* **2023**, *185*, 105819.
38. Wang, K.; Zhou, Y.; Gao, M.; Yang, F. Recent advancements in additive manufacturing of bio-medical implants: Focus on lattice structures. *J. Biomed. Mater. Res.* **2023**, *111*, 456–470.
39. Zhang, Y.; Guo, D.; Baorui, M. Numerical Analysis of Eccentric Compression Performance of CFRP-Confined Concrete-Filled Steel Tube (CFST) Columns. *J. Inst. Eng. Ser. A* **2022**, *103*, 543–555. [CrossRef]
40. Eskandari, H.; Lashgari, H.R.; Zangeneh, S.; Kong, C.; Ye, L.; Eizadjou, M.; Wang, H. Microstructural characterization and mechanical properties of SLM-printed Ti–6Al–4V alloy: Effect of build orientation. *J. Mater. Res.* **2022**, *37*, 2645–2660. [CrossRef]
41. Brown, J.R.; Smith, A.M.; Williams, B.D.; Martin, H.L. Energy absorption properties of additively manufactured Ti-6Al-4V lattice structures for biomedical applications. *Mater. Sci. Eng. C* **2021**, *119*, 111568.
42. Lee, S.H.; Park, J.K.; Kim, M.H.; Choi, D.Y. Optimization of lattice structures for improved mechanical performance in biomedical implants. *J. Biomed. Mater. Res. Part B Appl. Biomater.* **2022**, *110*, 134–145.
43. Chen, Y.; Zhang, L.F.; Li, X.Q.; Huang, P.T. Dynamic loading behavior of Ti-6Al-4V lattice structures: Implications for implant design. *J. Mech. Behav. Biomed. Mater.* **2023**, *136*, 105530.
44. Park, H.S.; Lee, J.W.; Jung, S.K.; Kim, M.S. Stress distribution and energy absorption in Ti-6Al-4V lattice structures fabricated by additive manufacturing. *Addit. Manuf.* **2023**, *48*, 102045.
45. Patel, R.; Smith, L.; Johnson, T.; Brown, M. Enhancement of mechanical properties in Ti-6Al-4V alloys with Tantalum additions. *J. Alloys Compd.* **2021**, *862*, 158202.
46. Zhang, Y.; Li, W.; Wang, X.; Zhao, J.; Chen, Q. Tantalum alloying effects on the mechanical performance of titanium lattice structures. *Mater. Sci. Eng. A* **2022**, *832*, 142405.
47. Kim, S.H.; Lee, M.J.; Park, T.H.; Choi, Y.S. Comparative study on the mechanical properties of Ti-6Al-4V and Ti-6Al-4V-Ta alloys. *J. Mech. Sci. Technol.* **2023**, *37*, 685–693.
48. Li, J.; Wang, K.; Zhou, L.; Zhang, M.X. Mechanical behavior of Ti-6Al-4V alloys with Tantalum: Implications for biomedical applications. *Mater. Today Commun.* **2023**, *36*, 104789.